1994A&A...284...91F

Astron. Astrophys. 284, 91–104 (1994)

ASTRONOMY AND ASTROPHYSICS

Rotational modulation and flares on RS Canum Venaticorum and BY Draconis stars

XVIII. Coordinated VLA, ROSAT, and IUE observations of RS CVn binaries*

David C. Fox[1], Jeffrey L. Linsky[1]***, Anthony Veale[1], Robert C. Dempsey[1], Alex Brown[1], James E. Neff[2], Isabella Pagano[3], Marcello Rodonò[3], Gordon E. Bromage[4]†, Martin Kürster[5], and Jürgen H.M.M. Schmitt[5]**

[1] Joint Institute for Laboratory Astrophysics, University of Colorado and National Institute of Standards and Technology, Boulder, CO 80309-0440, USA
[2] Department of Astronomy & Astrophysics, Pennsylvania State University, 525 Davey Lab, University Park, PA 16802, USA
[3] Istituto di Astronomia, Università degli Studi, and Osservatorio Astrofisico di Catania, Città Universitaria, Viale Andrea Doria 6, I-95125 Catania, Italy
[4] Rutherford Appleton Laboratory Chilton, Didcot, Oxon OX 11 0QX, UK
[5] Max-Planck-Institut für extraterrestrische Physik, Giessenbachstr., D-85740 Garching, Germany

Received 29 June 1993 / Accepted 22 September 1993

Abstract. As part of a coordinated program of multi-wavelength observations of RS CVn close binary systems, we observed 15 systems with the VLA and 10 systems with IUE, simultaneously or nearly simultaneously with the ROSAT All Sky Survey observations of these stars. Of the 22 systems observed with ROSAT, three were observed both by IUE and the VLA. The principal aim of this program was to check the validity of the existing empirical correlations between the radio and soft X-ray emissions of their coronae, and between the chromospheric/transition region and coronal emissions. Previous studies of these correlations were usually based on nonsimultaneous observations and thus might be biased by source variability.

Radio observations were made at 3.6, 6 and 20 cm. Of the 15 observed RS CVn systems, we detected 11 with $\geq 4\sigma$ confidence at one or more wavelengths. The IUE observations were made within the RIASS (ROSAT-IUE All Sky Survey) program. We present the results of the VLA observations, along with the corresponding subsets of the ROSAT PSPC X-ray and WFC XUV survey, and RIASS IUE observations.

We obtained an extended VLA/IUE/ROSAT simultaneous coverage of one system, TY Pyx, covering more than one orbital period. These observations reveal that the quiescent radio flux of TY Pyx is relatively constant over time scales of up to 7 hours, but that it did change by a factor of 3 over 24 hours, probably due to a flare on 1990 Nov 12. The UV, XUV and X-ray fluxes do not show large day-to-day or phase-related variability.

The observation of the decay phase of a radio flare on EI Eri, with no accompanying X-ray or XUV flare, suggests that the lack of a strong correlation between X-ray and radio flares previously noted for dMe flare stars holds for RS CVn systems as well. We suggest that the radio flare may have been due to a coherent emission process such as electron cyclotron emission.

The simultaneous measurements presented here provide a unique test of the general correlation between radio and soft X-ray luminosities, $L_{\rm radio} \sim L_x^m$ (Drake et al. 1989) with a power-law slope close to unity, which was previously derived using data obtained years apart. Our derived slopes are consistent with and thus support the general correlations between coronal and chromospheric/transition region emissions previously derived from nonsimultaneous measurements of a much larger sample of these variable sources. However, the importance of simultaneous measurements for accurate energy balance calculations is stressed.

Key words: stars: binaries: close – stars: coronae – stars: flare – radio continuum: stars – ultraviolet: stars – X-rays: stars

1. Introduction

The class of RS Canum Venaticorum (RS CVn) systems, originally defined by Hall (1976), is now thought to consist of binaries characterized by strong Ca II H and K emission, a hotter

Send offprint requests to: J.L. Linsky

* The IUE observations were collected at the ESA Satellite Tracking Station, Villafranca (Spain) and at the NASA Goddard Space Flight Center, Greenbelt, MD (USA).

** *Current address*: Department of Physics, Harvard University, Cambridge, MA 02138 (USA).
*** Staff Member, Quantum Physics Division, National Institute of Standards and Technology.
† *Current address*: Department of Physics, University of Central Lancashire, Preston, UK.

© European Southern Observatory • Provided by the NASA Astrophysics Data System

1994A&A...284...91F

star of spectral type F or G and luminosity class IV or V, a cooler star of spectral type G or K and luminosity class IV or V, and an orbital period of between one day and two weeks. Hall classified similar detached binaries with periods of less than one day as short-period RS CVn systems, and those with periods longer than two weeks, and possessing one component of spectral class G or K and luminosity class II–IV, as long-period RS CVn systems. Members of the three classes are now often referred to, without distinction, as RS CVn systems.

The Ca II emission from these stars indicates a high level of chromospheric activity. While only Ca II emission was a defining characteristic, the activity of RS CVn systems typically manifests itself in many other ways. RS CVn systems exhibit periodic or quasi-periodic brightness variations attributed to the presence of cool, dark starspots covering large fractions of the stellar photosphere (Byrne 1992; Eaton 1992). Enhanced emission is observed in chromospheric and transition-region lines in the ultraviolet, and there is evidence for concentrated bright regions analogous to solar plages (Neff 1992; Linsky 1992). Dark photospheric starspots and bright chromospheric/transition region plages sometimes appear spatially correlated (Rodonò et al. 1987), but not always (Pagano et al. 1992; Rodonò 1992). Measurements of thermal bremsstrahlung emission in soft X-rays indicate that components of RS CVn systems possess magnetically confined coronae with temperatures of roughly 10^6 to 5×10^7 K (Swank et al. 1981; Majer et al. 1986; Dempsey et al. 1993b). Finally, RS CVn systems show strong continuum radio emission at centimeter wavelengths, with "quiescent" luminosities typically between 10^{16} and 10^{17} erg s^{-1} Hz^{-1} (Mutel et al. 1987; Drake et al. 1989), and larger radio flares, both of which are generally attributed to nonthermal gyrosynchrotron emission from mildly relativistic electrons.

Drake et al. (1989) found that the 6 cm radio luminosity, L_6, and the soft X-ray luminosity, L_x, of RS CVn systems are statistically correlated. Given that the X-ray and radio emission are generally believed to be radiated by different populations of electrons (i.e., thermal and nonthermal electrons, respectively), the origin of the correlation was unclear. Also, because the available radio and X-ray observations were typically obtained years apart, it was not known whether L_6 and L_x vary in phase with each other. The previous nonsimultaneous observations indicated only that the mean values $\langle \log L_6 \rangle$ and $\langle \log L_x \rangle$ (as approximated by the mean of the logarithms of one or more measurements) for a large sample of systems are correlated. However, RS CVn systems exhibit a great deal of variability, particularly at X-ray and radio wavelengths, and any correlation between the variations of L_6 and L_x for a single system about their mean values could be confirmed only with simultaneous measurements. If such a correlation exists, it would suggest a close physical connection between the radio and X-ray emission, which might also account for the relationship between $\langle \log L_6 \rangle$ and $\langle \log L_x \rangle$ of different systems.

Also chromospheric and transition region activity indicators, such as mean Mg II and C IV emission line fluxes, respectively, appear to be correlated with coronal X-ray emission (Ayres et al. 1981; Walter 1982; Oranje et al. 1982). However, owing to the the variability of RS CVn systems at all wavelengths, simultaneous observations could provide new insight into the nature of the mechanism behind the observed correlation.

In pursuit of this objective, we have observed 15 RS CVn systems at centimeter wavelengths with the VLA and 10 systems with IUE simultaneously or nearly simultaneously with ROSAT X-ray and EUV observations obtained during the All Sky Survey phase of the mission. A preliminary report of these observations was presented by Linsky et al. (1992). Our relatively unbiased selection criterion for the VLA observations was the ability to observe several targets that happened to lie near the same ecliptic longitude and thus could be observed simultaneous with ROSAT within a few hours of each other. The targets selected for IUE observations tended to be the brighter systems. We measured radio fluxes at three wavelengths, 3.6, 6, and 20 cm, to obtain spectral information with which to constrain the characteristics of the source region.

The simultaneous ROSAT, IUE, and optical observations of 10 RS CVn systems, including three of those we observed also with the VLA, will be described in detail in subsequent papers (Neff et al. 1993; Kürster et al. 1993). These studies will be mainly concerned with rotationally induced variability due to surface inhomogeneities. The present paper addresses only correlations of averaged luminosities. However, we include here a more extended data set for TY Pyx, which was the subject of a major VLA-IUE-ROSAT coordinated observing campaign and will be described further in a companion paper (Neff et al. 1993). A preliminary report of the TY Pyx data was presented by Kürster et al. (1992). Ayres et al. (1993) have also completed a correlated IUE-ROSAT study of about 80 late-type stars.

2. Observations

The complete VLA-IUE-ROSAT observation log is presented in Table 1. Details on the observations with the different instruments and data reduction methods are given in the following subsections.

2.1. VLA observations

We obtained the radio observations from 1990 August to November using the NRAO Very Large Array.[1] We generally observed at 3.6, 6, and 20 cm, with the array divided into two subarrays to allow simultaneous measurements at two of the three wavelengths at any given time. At each wavelength, two 50 MHz bandpasses were used, with central frequencies 8465 and 8415 MHz (3.6 cm), 4885 and 4835 MHz (6 cm), and 1515 and 1465 MHz (20 cm). Table 2 summarizes the dates, array configurations, subarrays, and wavelengths of the individual observations. We flagged and calibrated the data, and made maps

[1] The VLA is a facility of the National Radio Astronomy Observatory which is operated by Associated Universities, Inc., under cooperative agreement with the National Science Foundation.

© European Southern Observatory • Provided by the NASA Astrophysics Data System

1994A&A...284...91F

Table 1. Observation log: the dates are included between 1990 August and 1991 January.

Name	Catalog No.		ROSAT PSPC	IUE	VLA
ζ And	HD	4502	Jan 3-4-5	Dec 31	...
LX Per	HD	19845	Aug 9-10	...	Aug 9
UX Ari	HD	21242	Aug 6-7	...	Aug 9
...	HD	22403	Aug 7-8-9	...	Aug 9
V711 Tau	HD	22468	Aug 1-2-3	Aug 2	...
EI Eri	HD	26337	Aug 8-9-10	...	Aug 9
...	HD	37824	Sep 6-7	...	Sep 6-7
TW Lep	HD	37847	Sep 3-4-5	...	Sep 6
...	HD	39576	Sep 8-9	...	Sep 7-8-9-10
SZ Pic	HD	39917	Sep 7-8-9	...	Sep 6-7-8-9-10-11
SV Cam	HD	44982	Sep 14-15	Sep 13	Sep 12
TY Pyx	HD	77137	Nov 10-11-12	Nov 10-11-12-13	Nov 9-10-11-12
DK Dra	HD	106677	Oct 22-23-24	Oct 21	...
IL Com	HD	108102	Dec 8-9	Dec 9	...
WW Dra	HD	150708	Jan 4-5-6-7-8-9-10	Jan 8	...
Z Her	HD	163930	Sep 11	Sep 11	Sep 12
V772 Her	HD	165590	Sep 12-13-14	...	Sep 12
AR Lac	HD	210334	Dec 11-12-13	Dec 12-13	...
λ And	HD	222107	Dec 31, Jan 1-2	Dec 31	...
CQ Aur	HDE	250810	Sep 11-12-13	...	Sep 11-12
MM Her	HDE	341475	Sep 11	...	Sep 12
RW UMa	...		Nov 11-12-13-14	...	Nov 10-11-12

Table 2. VLA array configurations

Dates	Array Configuration	Subarrays and Wavelengths
1990 Aug 9	B	2 (3.6/20 cm and 3.6/6 cm)
1990 Sep 6–7	B	2 (3.6/20 cm and 3.6/6 cm)
1990 Sep 8–11	B	2 (1 source per subarray, 3.6/6/20 cm)
1990 Sep 12	B	1 (array not divided, 3.6 cm only)
1990 Nov 9–12	C	2 (3.6/20 cm and 3.6/6 cm)

of the sources, using the NRAO Astronomical Image Processing System (AIPS) software. The observations during November used 3C286 as a primary flux calibrator, while the rest used 3C48. We "cleaned" those maps containing significant radio sources using the Cotton-Schwab algorithm as implemented in the AIPS routine MX.

For the 3.6 and 6 cm observations, we examined a circular region of radius 2″ around the optical position for radio sources with fluxes at least four times the r.m.s. noise level. We obtained optical positions and proper motions from the SAO Catalog for all of the targets, except RW UMa, for which we used the AGK 3 Catalog position. The SAO Catalog positions were checked against positions obtained from the Hubble Space Telescope Guide Star Catalog and found to agree to within 2″. We used the SAO positions in preference to the GSC positions, because the latter do not include annual proper motions, which, when integrated over the interval between position measurement and our observations, are significant.

At 20 cm, where the beam size exceeded our 2″ criterion, we checked for 4σ radio sources within the halfwidth of the beam from the expected position. For sources detected at 3.6 cm, we used the 3.6 cm position as our expected position at 20 cm.

In three cases, UX Ari, EI Eri, and TY Pyx, we found radio sources well above the 4σ detection threshhold (39–75 σ), but located 2 to 3″ from the SAO positions. We were fortunate to find precise astrometric radio and optical positions for UX Ari (Johnston et al. 1985) and for TY Pyx and EI Eri (White et al. 1990) which reduced the discrepancies to less than 1″, permitting reliable identifications of the radio sources with our target systems. In one other case, SZ Pic, a weak source was found between 2 and 3″ from the SAO position, with the exact position varying from day to day within the beam size, as is typical for weak sources. Drake et al. (1989) also noted a radio source at the same offset, within our resolution, from the SAO position. We therefore classify the source as a possible detection of SZ Pic.

The measured peak radio fluxes and upper limits are summarized in Tables 3 and 4. For those systems that were observed on two or more days but not detected on any individual day, the table entries reflect the combined data from all days, for maximum sensitivity.

© European Southern Observatory • Provided by the NASA Astrophysics Data System

1994A&A...284...91F

Table 3. VLA detections (with 1σ errors)

RS CVn System	1990 Date	Flux (mJy) 3.6 cm			6 cm			20 cm		
UX Ari	Aug 9	4.38	±	0.10	4.97	±	0.15	5.40	±	0.43
EI Eri	Aug 9	variable								
HD 22403	Aug 9	0.50	±	0.08	0.60	±	0.14		<	2.04
TW Lep	Sep 6	4.51	±	0.23	2.07	±	0.20	1.10	±	0.30[a]
HD 37824	Sep 6–7[b]	0.30	±	0.07		<	0.44		<	1.60
SZ Pic [c]	Sep 6	0.61	±	0.11	0.92	±	0.16		<	1.48
"	Sep 7	0.75	±	0.13	1.26	±	0.16		<	1.60
"	Sep 8		<	0.44		<	0.52		<	1.24
"	Sep 9		<	0.48		<	0.56		<	1.24
"	Sep 10		<	0.40	0.84	±	0.13		<	1.28
"	Sep 11	0.36	±	0.09	0.83	±	0.11		<	1.28
V772 Her	Sep 12	7.71	±	0.14		...			...	
MM Her	Sep 12	0.36	±	0.06		...			...	
Z Her	Sep 12	0.33	±	0.07		...			...	
SV Cam	Sep 12	0.41	±	0.07		...			...	
TY Pyx	Nov 9	2.22	±	0.09	2.39	±	0.22		<	5.2
"	Nov 10	1.43	±	0.06	1.36	±	0.08		<	3.2
"	Nov 11	1.54	±	0.06	1.40	±	0.08		<	3.0
"	Nov 12	4.48	±	0.06	4.56	±	0.10	4.33	±	0.47

[a] Marginal detection (3.7σ) but consistent with the 3.6 and 6 cm positions to within the resolution of the 20 cm observation.
[b] Nondetection ($< 4\sigma$) on each individual day.
[c] Possible detection, offset by 2 to 3" from SAO position, but consistent with the measured position of Drake, Simon, & Linsky (1989).

For the detected systems, we also measured the circular polarization. In Table 5, we list the circular polarizations detected for UX Ari, as well as 4σ upper limits where those limits are below 50%.

2.2. *ROSAT observations*

The ROSAT observations were obtained during the ROSAT All Sky Survey. During each 96 minute orbit, ROSAT scanned a great circle of ecliptic longitude, covering the entire sky in six months. Each source fell within the 2° diameter field of view of the PSPC for up to 30 s of each orbit over $\gtrsim 2$ days. For a more detailed description of the survey see Cruddace et al. (1989). The ROSAT PSPC (see Trümper 1984; Pfeffermann et al. 1987) is sensitive to X-rays in the energy range 0.1 – 2.4 keV. The WFC (Wells et al. 1990; Kent et al. 1990), with a 5° field of view, observed each source for up to 80 s of each orbit, over $\gtrsim 5$ days, alternating each day between two filters, S1A and S2A, with XUV bandpasses of 0.08 – 0.18 keV (67.5 – 152.5Å) and 0.06 – 0.11 keV (112.5 – 192.5Å), respectively.

Further details of the ROSAT PSPC and WFC observations of RS CVn systems, and the analysis of these X-ray and XUV observations, may be found in Dempsey et al. (1993a) and Brown et al. (1993), respectively. We note that the XUV luminosities were computed assuming the plasma temperatures derived by Dempsey et al. (1993b) in their analysis of PSPC All Sky Survey data and the XUV emissivities computed by Mewe et al. (1985, 1986).

2.3. *IUE observations*

The IUE observations were scheduled within the RIASS program so as to obtain at least one SWP (1150–1950 Å) low-dispersion and one LWP (2000–3200 Å) high-dispersion spectrum at or near the times when each target was observed by ROSAT during the All Sky Survey. The IUE spectra are listed in Table 6. Only for TY Pyx and AR Lac was sufficient IUE time allocated to cover an entire orbital period or more. For TY Pyx, each SWP spectrum consisted of three exposures at the same offset to include exposure time while the individual LWP spectra were being "read down." Thus, while the cumulative exposure in each SWP spectrum was 90 to 120 minutes, the effective time resolution was approximately 6 hours. For the complete IUE observation log of these two systems, the reader is referred to the papers by Neff et al. (1993) and Kürster et al. (1993).

The IUE spectra were extracted and calibrated with the standard IUE RDAF routines. In Table 7 we report the integrated fluxes at Earth derived by integrating the corresponding features using a local background continuum defined on each side of the line. A complete description of the IUE data analysis can be found in the two above-quoted papers on the TY Pyx and AR Lac extended data sets. For these two systems, only phase-

© European Southern Observatory • Provided by the NASA Astrophysics Data System

1994A&A...284...91F

Table 4. Upper limits (4σ)

RS CVn System	1990 Date	Flux (mJy) 3.6 cm	6 cm	20 cm
LX Per	Aug 9	< 0.28	< 0.40	< 1.08
HD 39576	Sep 7–10	< 0.32	< 0.38	< 0.92
CQ Aur	Sep 11–12[a]	< 0.22	< 0.48	< 0.72
RW UMa	Nov 10–12[b]	< 0.16	< 0.64	< 1.76

[a] On 12 September, observations were made only at 3.6 cm.
[b] Observations at 6 and 20 cm were made only on 11 November.

Table 5. Circular polarization and 4σ upper limits

RS CVn System	1990 Date	% Circular Polarization (+ is RCP) 3.6 cm	6 cm	20 cm
UX Ari	Aug 9	-25 ± 2	-18 ± 3	$-18 < 22$
TW Lep	Sep 6	< 19	< 44	...
V772 Her	Sep 12	< 5	...	...
TY Pyx	Nov 9	< 17	< 33	...
"	Nov 10	< 17	< 21	...
"	Nov 11	< 15	< 22	...
"	Nov 12	< 5	< 9	< 20

Table 6. Log of the RIASS IUE observations

Star	HD No.	Image	Disp.	Date (UT)	UT Start Time *hh:mm*	Exp. Time *min*	Phase mid. exp.
ζ And	4502	SWP 40501	low	1990 Dec 31	04:07	20	0.581
"		LWP 19501	high	1990 Dec 31	03:31	15	0.579
"		LWP 19502	high	1990 Dec 31	04:33	10	0.582
V711 Tau	22468	SWP 39386	low	1990 Aug 03	02:23	30	0.913
SV Cam	44982	SWP 39634	low	1990 Sep 14	06:09	100	0.105
TY Pyx[a]	77137						
DK Dra	106677	SWP 39889	low	1990 Oct 21	01:20	75	0.551
"		LWP 19045	high	1990 Oct 21	00:11	30	0.550
IL Com	108102	SWP 40294	low	1990 Dec 09	14:54	120	0.163
"		LWP 19378	low	1990 Dec 09	16:06	280	0.273
WW Dra	150708	SWP 40549	low	1990 Dec 08	08:46	100	0.835
"		LWP 19524	high	1990 Dec 08	12:15	303	0.882
Z Her	163930	SWP 39613	low	1990 Sep 12	00:48	120	0.860
"		LWP 18763	high	1990 Sep 12	02:38	90	0.876
AR Lac[b]	210334						
λ And	222107	LWP 19500	high	1990 Dec 31	01:35	4	0.629
"		SWP 40500	low	1990 Dec 31	02:03	30	0.630

[a] See Neff et al. (1993).
[b] See Kürster et al. (1993)

averaged fluxes, outside of flare and eclipse phases, are given in Table 7.

3. Results

3.1. Spectral characteristics of the radio emission

In Table 8, we list the spectral indices α (defined by $S_\nu \propto \nu^\alpha$) and their $\pm 1\sigma$ errors for those stars detected at multiple wavelengths. Three of these stars, UX Ari, HD 22403, and TY Pyx, exhibit spectra that are flat or slightly decreasing with increasing frequency, consistent with previous observations of quiescent emission (Mutel et al. 1987). There are several possible explanations for flat spectra in terms of gyrosynchrotron emission. Optically thin gyrosynchrotron emission from a homogeneous source of electrons with a power-law energy distribution will produce such spectra for small power-law indices $\delta \lesssim 3$ (Dulk

© European Southern Observatory • Provided by the NASA Astrophysics Data System

1994A&A...284...91F

Table 7. Integrated net emission line fluxes at Earth in units of 10^{-13} erg s^{-1} cm^{-2} for the RS CVn systems in Table 6.

Star	C III	N V	O I (a)	C II	O I (b)	Si IV	C IV	He II	C I + [O III]	Si II	Al III	Si III] + ... + S I	Mg II *k*	Mg II *h*
ζ And	3.3	8.1	30.1	10.6	4.9	10.7	21.2	9.1	8.7	21.9	3.7	13.6	505.5	348.0
V711 Tau	11.4	5.0	16.0	24.6	...	8.6	37.1	19.3	8.2	15.2	...	0.27	...	...
SV Cam	...	...	...	...	...	...	1.0	...	...	...	...	...	...	...
TY Pyx	1.3	1.5	1.8	3.7	...	2.2	8.7	1.8	2.1	2.6	0.7	0.9	32.4	23.5
DK Dra	1.5	3.3	6.8	2.8	...	2.7	12.9	2.4	3.1	5.4	...	2.4	99.3	70.8
IL Com	...	0.8	...	1.0	0.7	0.8	2.1	1.0	1.2	...	...	...	9.3	5.8
WW Dra	...	0.2	0.3	0.9	...	...	0.8	0.7	0.6	1.3	...	...	7.9	7.4
Z Her	0.2	0.4	0.4	0.8	...	0.8	2.2	0.9	1.5	...	*abs*	...	13.7	11.3
AR Lac	3.4	3.3	5.4	8.0	2.2	4.5	22.3	7.0	5.0	7.3	2.5	2.3	87.0	65.9
λ And	5.4	3.9	41.0	13.7	5.3	12.5	24.8	15.9	17.9	29.3	5.2	11.2	793.0	593.0

Line identification: C III: 1175 Å; N V: 1239-1243 Å; O I(a): 1302-1305-1306 Å; C II: 1334-1336 Å; O I(b)+C I: 1356 Å(blended); Si IV: 1394-1403 Å; C IV: 1548-1551 Å; He II+Fe II: 1640 Å(blended); C I: 1658 Å + [O III]: 1658-1661 Å; Si II: 1808-1817 Å; Al III+Fe III: 1855 Å(blended); Si III]: 1892 Å+ S I: 1900 Å + C III]: 1909 Å + S I: 1915 Å; Mg II *k*: 2795.5 Å; Mg II *h*: 2802.7 Å

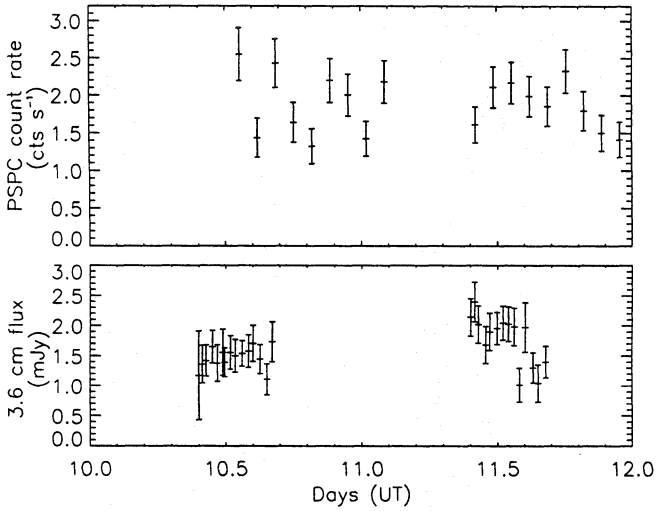

Fig. 1. 3.6 cm radio fluxes, averaged over 10 minute intervals, with 1σ uncertainties, and X-ray (PSPC) count rates for TY Pyx, 1990 November 10-12 UT

Table 8. Radio spectral indices ($S_\nu \propto \nu^\alpha$)

RS CVn System	1990 Date	$\alpha_{3.6-6}$	α_{6-20}
UX Ari	Aug 9	-0.25 ± 0.07	-0.07 ± 0.07
HD 22403	Aug 9	-0.14 ± 0.26	...
TW Lep	Sep 6	$+1.50 \pm 0.20$	$+0.50 \pm 0.30$
SZ Pic	Sep 6	-0.80 ± 0.56	...
"	Sep 7	-1.02 ± 0.47	...
"	Sep 11	-1.64 ± 0.65	...
TY Pyx	Nov 9	-0.14 ± 0.21	...
"	Nov 10	$+0.10 \pm 0.15$	...
"	Nov 11	$+0.20 \pm 0.14$	...
"	Nov 12	-0.03 ± 0.05	$+0.04 \pm 0.10$

& Marsh 1982; Massi & Chiuderi Drago 1992). However, since flat spectra seem to be the rule for quiescent emission, this explanation requires a physical mechanism that predicts small values of δ when the radio flux is low and the star is not flaring. In fact, small values of δ, and hence significant numbers of very energetic electrons, are expected during flares rather than during quiescent periods (Morris et al. 1990). It is more likely that the flat spectra are indicative of emission from a number of different source regions with different physical characteristics, as illustrated in Mutel et al. (1987). For example, the nonthermal synchrotron emission models of Chiuderi Drago & Franciosini (1993) show that flat spectra persist for many days after a flare, since initially synchrotron radiation from relativistic flare electrons in a compact set of loops with high magnetic fields dominates but subsequently the observed low flux emission (often called quiescent emission) is primarily from a more extended region with smaller magnetic fields. Their model is consistent with the core-halo model of Mutel et al. (1985).

We note that in Table 8 one star, TW Lep, shows large positive spectral indices and another star, SZ Pic, shows large negative spectral indices. Also the observed 6-cm fluxes are well above the quiescent values for those stars cited by Drake et al. (1989, 1992). These spectral indices can be explained within the framework of the core-halo model of Mutel et al. (1985). Large positive values of α can occur early during a radio flare when the compact source is very optically thick at centimeter wavelengths and synchrotron self-absorption is important. On the other hand, large negative values of α can occur when the emission late in a flare is dominated by an optically thin halo source and δ is large indicating that the electron energy distribution has lost most of its high energy component.

3.2. The variability of TY Pyx quiescent emission

The nature of quiescent radio emission from RS CVn stars remains an open question. We shall use the term "quiescent emis-

© European Southern Observatory • Provided by the NASA Astrophysics Data System

1994A&A...284...91F

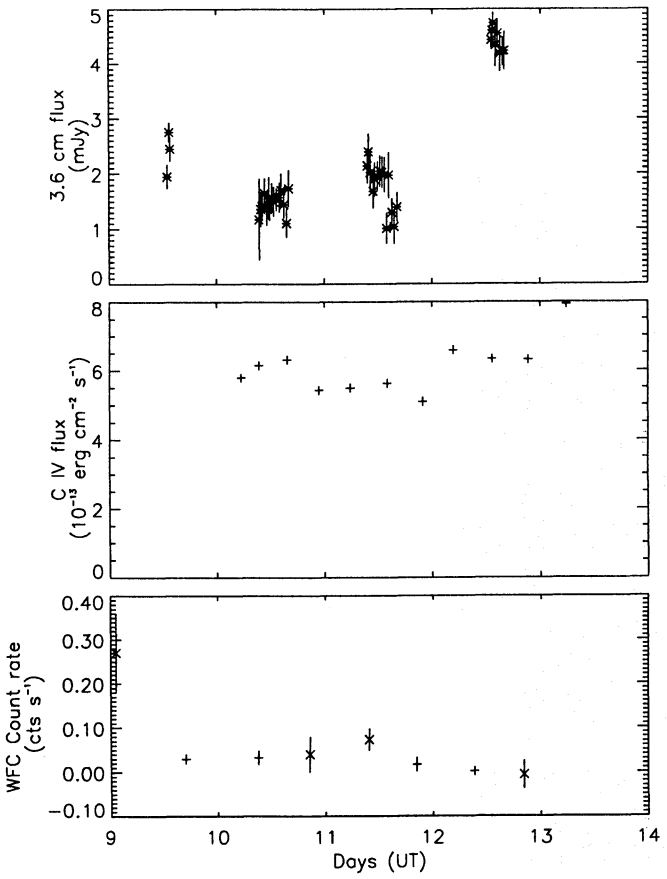

Fig. 2. Simultaneous 3.6 cm radio and C IV fluxes, and daily averages of the WFC count rates (+ for filter S1A, × for filter S2A), for TY Pyx, 1990 November 9 – 13 UT

sion" in the sense of low-level, slowly varying emission. A stricter definition might require in addition that the star reaches its minimum radio flux level before the radio emission could be called quiescent. However, such a minimum level is difficult to identify reliably without long-term observations of the star in question, and emission at this level may not be qualitatively different from emission meeting our less strict definition. In order to examine the nature of quiescent emission, we have plotted in Figs. 1 and 2 the 3.6 cm flux of TY Pyx as a function of time. The light curve shows no evidence of radio flares on time scales of a few hours or less. We do, however, find flux variations of up to a factor of 3 between consecutive days, much greater than the variations within each day's observations, which last up to 7 hours. Quantitatively, the r.m.s. variations of the average daily fluxes were 51% of the mean for the 4 days, while the r.m.s. variations of 10 minute averages within each day, about the mean for that day, ranged from 14 to 28%. Since measurements for even a constant source will show an r.m.s. variation equal to the uncertainty σ_{meas} in the measurement, the actual variability $\sigma_{\rm corr}$ is $(\sigma^2 - \sigma^2_{\rm meas})^{1/2}$. This corrected r.m.s. variation ranged from 13 to 19% for the 10 minute averages, while for the daily averages the correction was negligible.

The higher fluxes on the first and last days (Nov 9 and 12) could be attributed to small flares rather than to quiescent emission. However, at least on Nov 12 when our observations extend over 2.9 hours, the radio flux was relatively constant. The maximum and minimum fluxes, 4.74 ± 0.20 mJy and 4.18 ± 0.33 mJy differ by only 1.5σ, and a least-squares fit assuming exponential decay gives a timescale of 36^{+37}_{-8} hours. This could be either a long duration flare occurring after the end of the PSPC observations or a flare at that time which rose, remained constant for at least 3 hours, and then decayed more rapidly after the end of our observations.

The alternative hypothesis is that the slowly varying emission observed on Nov 12, as well as that on Nov 9, represents quiescent emission. Under this assumption, we see that the quiescent emission from TY Pyx varies only slightly about the mean over timescales of up to 7 hours, but shows large day-to-day variations. This would have implications for various models of the origin of quiescent emission. For example, consider the frequently proposed hypothesis that the slowly varying quiescent emission level is composed of a large number of small flares overlapping in time. Assuming that the flares occur at a certain average rate r, and that the probabilities of individual flare events are uncorrelated, we see that the number of flares N occurring in a time interval of length t will follow a Poisson distribution with mean $\overline{N} = rt$, as long as t is greater than the duration of an individual flare. Since the r.m.s. variations of a Poisson distribution as a fraction of the mean are of order $\overline{N}^{-1/2} \propto t^{-1/2}$, we would expect larger fractional variations on smaller time scales. In fact, we see the exact opposite. This implies either that the small flare duration is of the order of several hours, so a fairly constant level is maintained over our 7 hour observations, or that there is some correlation between individual flares over that time scale.

A portion of the slower variation could be attributed to rotational modulation of the radio-emitting plasma onto and off the visible hemisphere, since the average flux was higher on the first and last days of observation, which were separated by 3.05 days, nearly the full 3.2 day period of TY Pyx. However, the flux on these two days differed by a factor of 2 so that if we were to assume rotational modulation of an active region, then we must still explain the intrinsic variations on a time scale of several days.

Unfortunately, the ROSAT PSPC observations of TY Pyx covered only the two middle days of the radio observations, over which time interval there was little evidence of variability in either the radio or X-ray emission (see Fig. 1). Thus, we were unable to use this case to decide whether variations in the quiescent radio and X-ray emission of an individual system are correlated. The 3.6 cm radio fluxes, C IV fluxes obtained with IUE, and the ROSAT WFC count rates in each filter (S1A and S2A), averaged over the orbits in each day, are shown in Fig. 2. While the WFC observations span the entire 4 days of the radio observations, the poor signal-to-noise ratio of the daily averages makes it difficult to draw any conclusions about variability of the XUV emission. The absence of large flux enhancements in the C IV and XUV bands and the inadequacy of the rota-

© European Southern Observatory • Provided by the NASA Astrophysics Data System

1994A&A...284...91F

tion modulation hypothesis lead us to the conclusion that the enhanced radio flux on Nov. 12 was probably due to a flare.

3.3. A flare on EI Eri

Our radio observations of EI Eri clearly show the decay phase of a flare (see Fig. 3). The peak of the flare occurred before 12:00 UT, 1990 August 9, and probably before 10:30 UT when our observations began. The peak flux at 3.6 cm was at least 20 mJy. By the end of our observations at 18:30, it had dropped to 0.4 ± 0.7 mJy, suggesting a 4σ upper limit on the post-flare quiescent flux of < 2.8 mJy. There does not appear to be any evidence of a flare decay in the X-ray or XUV data. On the contrary, the PSPC and WFC count rates gradually increased during the period of the radio observations. The absence of an obvious correlation between centimeter emission and X-rays in specific flare events has previously been noted in observations of dwarf flare stars (Karpen et al. 1977; Kundu et al. 1988). On the other hand, X-ray monitoring of σ^2 CrB (Stern et al. 1992) revealed a simultaneous X-ray and radio flare, as well as two other X-ray peaks whose rough coincidence with longer duration increases in radio flux may or may not indicate an actual relationship between the two.

The 20 cm flux of 8.8 mJy at the start of the observation was $51 \pm 6\%$ right circularly polarized, while the 6 cm flux of 14 mJy was $20 \pm 3\%$ right circularly polarized, and the 3.6 cm flux had a possible average right circular polarization (3.3σ) of $5 \pm 1.5\%$. The polarization at 6 and 20 cm seemed to decline with time, although after 12:00 UT the total flux levels were too low for accurate polarization measurements. The 3.6 and 6 cm fluxes appeared to decay exponentially with time scales τ of 4.5 ± 0.8 hr and 4.3 ± 0.5 hr, respectively. The time scale for decay of the 20 cm emission, $\tau = 4.3 \pm 2.6$ hr, though uncertain due to the smaller number of measurements, is consistent with the 3.6 and 6 cm flux decay time scales. We note that Mutel et al. (1987) also detected large values of circular polarization (30 – 78%) from another RS CVn system HR 1099.

We should note that there was some difficulty in the analysis of the 6 cm data on EI Eri. On the longest baselines of $\sim$ 100–170 kλ, the image appeared resolved into two distinct sources separated by 2″. Both sources decreased in flux from 6–8 mJy, resembling the flare decay seen at the other two frequencies, so a confusing source is ruled out. Since such a double source was not seen at 3.6, where it could also have been resolved, and more importantly, since 2″ would correspond to a separation of 2×10^{15} cm at a distance of 75 parsecs (Fekel et al. 1987), which would be an implausibly large source size for an RS CVn, the data from the longest baselines were assumed to be corrupted. Therefore, only baselines of ≤ 40 kλ were used in finding the fluxes cited above as well as those shown in Fig. 3. An examination of the calibrated visibilities from the first observation of EI Eri at 10:30 UT as a function of baseline length confirmed that the real part was constant at $\sim$ 14 mJy for baselines $\lesssim 50$ kλ, while for longer baselines the visibilities were extremely erratic. Thus we are reasonably confident that the fluxes obtained from the baselines of shorter than 40 kλ are accurate.

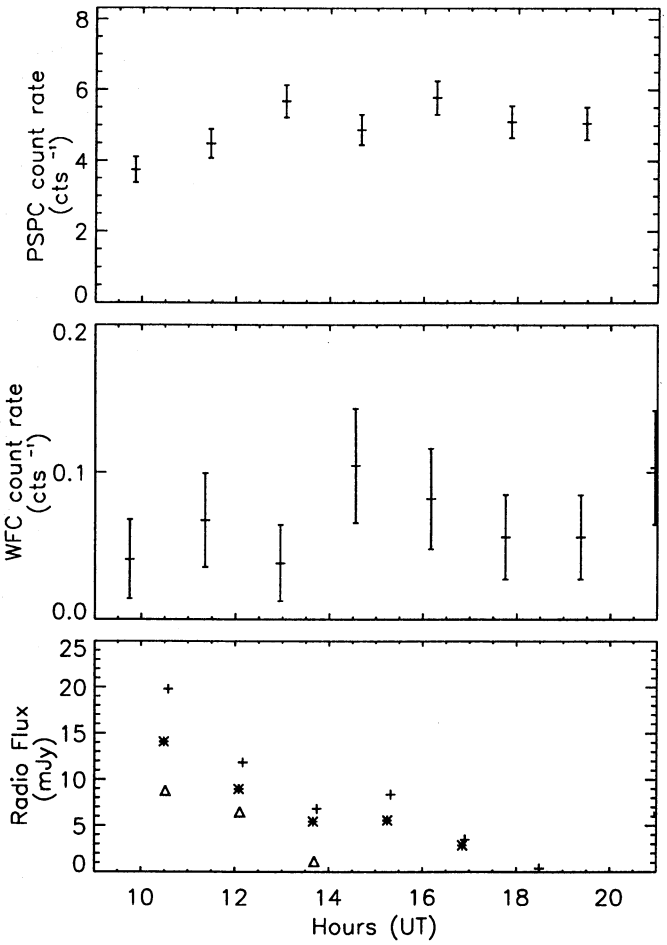

Fig. 3. Radio fluxes at 3.6 cm (+), 6 cm (*), and 20 cm (△), as well as ROSAT PSPC and WFC count rates (filter S1A) for EI Eri, during the observed radio flare

Fekel et al. (1987) have made spectroscopic observations of EI Eri and have deduced various parameters of the system. They measured values for the mass function $f(m) \equiv (M_2 \sin i)^3/(M_1+M_2)^2 = 0.0041$ and for the line-of-sight component of the semimajor axis of the orbit of the primary star, $a_1 \sin i = 7.29 \times 10^{10}$ cm. Using these values, as well as their constraints on M_1 and on M_1/M_2, we find that the two stars are separated by a distance a, with $6.9R_\odot \leq a \leq 8.9R_\odot$. Adopting a value of $a = 7.9R_\odot$, assuming a spherical radio source region of diameter a, and using $d = 75$ parsecs (Fekel et al. 1987), we calculate brightness temperatures of T_b (3.6 cm) = 2.1×10^9 K, T_b (6 cm) = 4.1×10^9 K, and T_b (20 cm) = 2.9×10^{10} K at the start of our observations. The values of T_b at the flare peak may have been even larger.

First, we consider whether the observed flare may be explained as gyrosynchrotron emission from mildly relativistic electrons. The brightness temperature of incoherent emission is limited by the effective temperature $T_{\rm eff}$ of the emitting electrons. Using the formulas of Dulk & Marsh (1982) for power-

© European Southern Observatory • Provided by the NASA Astrophysics Data System

1994A&A...284...91F

law electrons, we see that the maximum value of $T_{\rm eff}$, achieved when $\delta = 2$, $\theta = 20°$ and $\nu/\nu_B = 100$, is 1.9×10^{10} K. Therefore, to account for the emission at 20 cm, an emitting region of diameter $9.75R_\odot = 1.24a$ would be required. However, for the 20 cm emission to have the observed degree of circular polarization, ν/ν_B must be ≤ 30 (Dulk 1985), again assuming $\delta = 2$, and therefore, $T_{\rm eff}$ must be $\leq 8.6 \times 10^9$ K. Moreover, in this case, the optical depth τ must be $\ll 1$, and thus $T_b = \tau T_{\rm eff}$ would be even smaller. Adopting $\tau = 1/5$ as a generous upper limit on the optical depth for which the circular polarization formula of Dulk (1985) would hold, we find that $T_b(20{\rm cm}) \leq 1.7 \times 10^9$ K. Therefore, a gyrosynchrotron radio source would require a diameter of $32.6R_\odot \approx 4a$, or an area of roughly $12.6a^2$. This is different from the picture suggested by VLBI observations of UX Arietis and Algol at shorter wavelengths (e.g., Mutel et al. 1985) in which emission is observed from both from a compact core (smaller than the stellar photosphere) and a halo with an area approximately four times the square of the system size.

A more plausible alternative to a gyrosynchrotron explanation of the flare is a coherent mechanism, such as plasma emission or electron cyclotron maser emission. A coherent mechanism for the radio emission, in which a small number of electrons radiate efficiently, would also naturally account for the lack of a corresponding X-ray flare. Plasma emission is not expected to escape at frequencies above 1 GHz (Melrose 1987). Electron cyclotron maser emission occurs at harmonics of the cyclotron frequency. Direct maser emission is expected to be restricted to the first or second harmonic, since these modes would grow most rapidly, extracting all the free energy from the electron distribution and thus suppressing higher modes (Dulk 1985), although indirect mechanisms may be able to produce somewhat higher harmonics (Melrose 1991). If the observed flare were due to electron cyclotron maser emission at the second harmonic of the cyclotron frequency, then a field of 1500 G would be required to account for the emission at 3.6 cm. This implies an emission region close to the stellar photosphere, if the radio emission originated in magnetic loops emerging from starspots with field strengths similar to typical solar values of 3500 G. The association of flare emission with starspots and the assumed starspot field strength are both plausible, but not yet supported by observations.

3.4. Correlation of radio and X-ray emission

As shown by our EI Eri data and by observations of other stars, flares at either X-ray or radio wavelengths are typically not accompanied by significant variability at the other wavelength band. Whether variations in quiescent radio and X-ray emission show correlation is uncertain. Doyle et al. (1992) noted that a steady increase in 6 cm flux from II Peg was accompanied by a steady increase in X-ray flux measured by GINGA, and a steady decrease in radio flux the next day was accompanied by a steady decrease in X-ray flux. In other cases (e.g., Stern et al. 1992), the correspondence is less clear. It is difficult to give a definite answer to the question of correlation of nonflaring radio and

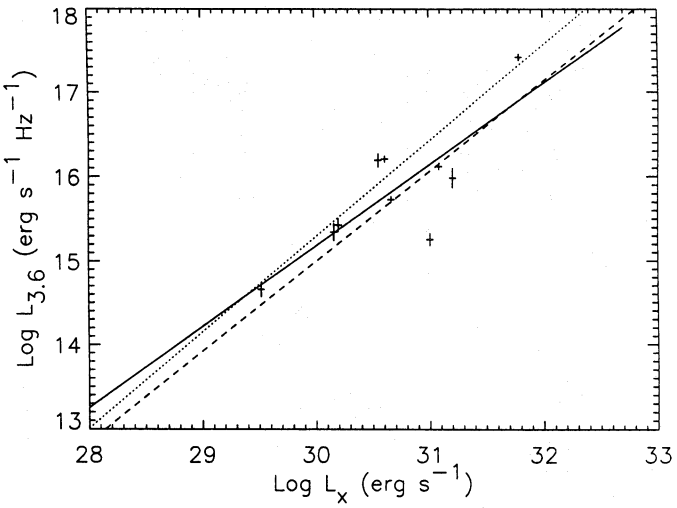

Fig. 4. $L_{3.6}$ versus L_x (from ROSAT PSPC) for the stars detected at 3.6 cm, excluding EI Eri. The solid line is a least-squares fit to the simultaneous values of log $L_{3.6}$ and log L_x shown. The dashed line is the analogous maximum-likelihood fit (Drake 1992) to the nonsimultaneous data of Drake et al. (1989, 1992). The dotted line is the maximum-likelihood fit to the nonsimultaneous data of Dempsey et al. (1993a)

X-ray emission without more extended simultaneous observations of individual systems. However, it may still be possible to gain some insight into the nature of the correlation between radio and X-ray emission noted by Drake et al. (1989) using observations of different systems. In order to do so, we must compare the relationship between radio and X-ray luminosities derived from nonsimultaneous measurements with that derived from our simultaneous observations.

In Table 9, we list the 3.6 cm luminosities of the systems we detected, along with the simultaneous or nearly simultaneous ROSAT X-ray luminosities from Dempsey et al. (1993a). The luminosities are based on distances from Strassmeier et al. (1988). The stated uncertainties do not include any uncertainties in the distances.

In Fig. 4, we have plotted the 3.6 cm luminosity $L_{3.6}$ against the X-ray luminosity L_x on a log-log scale for the 10 detected systems. EI Eri was not included because there was no correspondence during the flare between the radio and X-ray luminosities and quiescent radio emission at the end of the flare was below the detection threshhold. The solid line is an unweighted least-squares fit to our sample, corresponding to $L_{3.6} \sim L_x^{0.96\pm0.24}$.

The dashed line represents the maximum-likelihood fit $L_6 \sim L_x^{1.07\pm0.14}$ (Drake 1992) to the nonsimultaneous data presented by Drake et al. (1989, 1992), excluding systems with $\log L_x < 29.45$ which could be active single stars misidentified as RS CVn systems (Drake 1992). The dotted line is the maximum-likelihood fit $L_6 \sim L_x^{1.14\pm0.19}$ to the nonsimultaneous ROSAT PSPC and VLA data reported by Dempsey et al. (1993a). The maximum-likelihood method used to obtain these two fits, which allows the inclusion of upper limits as well as detections, is described in Drake et al. (1989). While the latter

© European Southern Observatory • Provided by the NASA Astrophysics Data System

1994A&A...284...91F

Table 9. X-ray, XUV, UV and radio luminosities of the RS CVn systems.

RS CVn System	HD No.	Distance (pc)	L_{bol}[d] (10^{34} ergs s^{-1})	L_x (10^{30} ergs s^{-1})	L_{S1} (10^{30} ergs s^{-1})	L_{S2} (10^{30} ergs s^{-1})	$L_{C\ IV}$ (10^{30} ergs s^{-1})	$L_{Mg\ IIh+k}$ (10^{30} ergs s^{-1})	$L_{3.6}$ (10^{15} erg s^{-1} Hz^{-1})
ζ And	4502	31	9.73	1.17	0.13	0.26	0.24	9.80	-
LX Per	19845	145	3.84	7.65	ND[b]	ND	-	-	<7.04
UX Ari	21242	50	2.51	12.0	0.91	0.72	-	-	13.1 ± 0.3
	22403	55	0.86	10.1	0.89	0.79	-	-	1.82 ± 0.29
V711 Tau	22468	36	2.43	23.77	1.26	1.07	0.57	-	-
EI Eri[a]	26337	75	2.87	13.8	1.38	1.45	-	-	74.2 ± 60.8
	37824	164	15.17	15.9	ND	ND	-	-	9.68 ± 2.26
TW Lep	37847	220	28.66	61.3	5.67	<4.05	-	-	262 ± 13
	39576	85	0.52	0.83	ND	ND	-	-	<2.76
SZ Pic[c]	39917	30.0	0.20	0.330	ND	ND	-	-	0.454 ± 0.086
SV Cam	44982	74	0.78	1.60	ND	ND	0.06	-	2.69 ± 0.46
TY Pyx[c]	77137	55	1.82	4.63	0.63	0.78	0.31	2.02	5.39 ± 0.22
DK Dra	106677	130	25.46	24.06	ND	ND	2.61	34.36	-
IL Com	108102	86	1.18	2.95	0.87	ND	0.19	1.33	-
WW Dra	150708	180	5.75	15.51	ND	ND	0.31	5.93	-
Z Her	163930	75	2.26	1.46	ND	ND	0.15	1.68	2.23 ± 0.47
V772 Her	165590	41.7	0.46	4.06	0.46	<0.51	-	-	16.1 ± 0.3
AR Lac	210334	40	1.98	10.55	1.27	2.07	0.43	2.92	-
λ And	222107	23	5.34	3.72	0.46	0.64	0.16	8.76	-
CQ Aur	250810	220	3.98	1.32	ND	ND	-	-	<12.73
MM Her	341475	190	2.19	3.56	ND	ND	-	-	15.6 ± 2.6

[a] The uncertainty in $L_{3.6}$ reflects the range of fluxes seen over the decay of the radio flare.
[b] ND = Not Detected
[c] The average 3.6 cm fluxes over the days for which there were ROSAT PSPC observations were used in computing $L_{3.6}$.
[d] The bolometric luminosities, except for HD 39576, are taken from Drake, Simon & Linsky (1989) but have been scaled to the distances from Strassmeier et al. (1988) and given in the third column.

two relations are both derived from 6 cm radio luminosities, we felt that comparison with our 3.6 cm data was more useful, because of the smaller number of systems we detected at 6 cm. As mentioned above, RS CVn quiescent spectral indices are generally relatively flat or slightly negative, so that we expect the relation of $\log L_6$ and $\log L_x$ to be shifted slightly upward with respect to the relation of $\log L_{3.6}$ and $\log L_x$ in Fig. 4. However, for spectral indices $-1 \leq \alpha \leq 1$, the shift was less than 0.22 in the logarithm of L_{radio}. The observed correlation of spectral index with luminosity (Mutel et al. 1987) will also tend to make the slope of the 6 cm relation smaller than that of the 3.6 cm relation, but this should have only a minor effect over the small range of luminosities in our sample. Given the small size of our sample, and the correspondingly large uncertainty in the slope of the relation, these effects should be negligible.

The slope of the relationship derived from simultaneous observations agrees to within 1σ with both of the previously stated relations for nonsimultaneous data. This is to be expected, so long as the correlation of $\langle \log L_{\rm radio} \rangle$ and $\langle \log L_x \rangle$, deduced from nonsimultaneous measurements, is more important than the deviations from the mean luminosities. We would expect a significantly different slope for simultaneous and nonsimultaneous relationships at the same radio frequency only if (a) $\Delta \log L_{\rm radio}$, defined as $\log L_{\rm radio} - \langle \log L_{\rm radio} \rangle$, and $\Delta \log L_x$, defined as $\log L_x - \langle \log L_x \rangle$, for individual systems were strongly correlated, (b) this correlation had a slope significantly different from that of the correlation of mean quantities, and (c) the ranges of $\Delta \log L_{\rm radio}$ and $\Delta \log L_x$ for individual systems were significant fractions of the ranges of $\langle \log L_{\rm radio} \rangle$ and $\langle \log L_x \rangle$ over the sample of systems observed.

A quantity that is more sensitive to the possible correlation of $\Delta \log L_{\rm radio}$ and $\Delta \log L_x$ is the r.m.s. scatter σ of simultaneous measurements about the relationship between $\log L_{\rm radio}$ and $\log L_x$. For nonsimultaneous measurements, this scatter has three independent components, which add in quadrature. There is a contribution from the scatter of individual systems about the relationship of $\langle \log L_{\rm radio} \rangle$ and $\langle \log L_x \rangle$ for different systems. Systems with the same mean X-ray luminosity can have different mean radio luminosities, and vice versa. In addition, there are contributions from the variations $\Delta \log L_{\rm radio}$ and $\Delta \log L_x$ for each system. Even if $\Delta \log L_{\rm radio}(t)$ and $\Delta \log L_x(t)$ are correlated, measurements at widely separated times t should not be. Thus for nonsimultaneous measurements, these two contributions to the scatter must add in quadrature as independent random quantities.

For simultaneous measurements, the scatter due to independent variations of $\langle \log L_{\rm radio} \rangle$ and $\langle \log L_x \rangle$ for different systems is the same as for nonsimultaneous measurements. However, the contributions to the scatter from $\Delta \log L_{\rm radio}$ and $\Delta \log L_x$ may differ for simultaneous measurements. If $\Delta \log L_{\rm radio}$ and $\Delta \log L_x$ are uncorrelated, their contributions to the scatter are the same as in the nonsimultaneous case. If they are perfectly correlated, and obey a relationship $\Delta \log L_{\rm radio} = m \Delta \log L_x$ with the same slope m as the relationship of $\langle \log L_{\rm radio} \rangle$ and $\langle \log L_x \rangle$, then the contribution due to variations $\Delta \log L_{\rm radio}$ and $\Delta \log L_x$ will be reduced to zero. In intermediate cases, the contribution from $\Delta \log L_{\rm radio}$ and $\Delta \log L_x$ will be less for simultaneous measurements than for nonsimultaneous measurements to the extent that $\Delta \log L_{\rm radio}$ and $\Delta \log L_x$ are correlated and to the extent that the slopes are the same.

In the above discussion we have used the term scatter somewhat loosely. To determine whether the empirical values of the scatter for simultaneous and nonsimultaneous measurements differ, we adopt the definition $\sigma \equiv [(1/N) \sum (\log L_{\rm radio}^{\rm meas} - \log L_{\rm radio}^{\rm pred})^2]^{1/2}$, where the sum is over a sample of N systems, $L_{\rm radio}^{\rm meas}$ represents the measured radio luminosity, and $L_{\rm radio}^{\rm pred}$ is the radio luminosity predicted from the measured X-ray luminosity and a linear least-squares fit of $\log L_{\rm radio}$ as a function of $\log L_x$. Because the slopes of the different least-squares fits we consider are similar, a different definition of the r.m.s. scatter σ would not greatly change our results.

© European Southern Observatory • Provided by the NASA Astrophysics Data System

1994A&A...284...91F

Using this definition, we find that the scatter $\sigma_{\rm sim}$ of our ten simultaneous measurements about their best fit is 0.40, corresponding to a variation of a factor of 2.5 in $L_{\rm radio}$. The r.m.s. scatter due to uncertainties in the measurement of the radio fluxes is 0.07. However, since independent contributions to the scatter add in quadrature, only 1.5% of $\sigma_{\rm sim}$ is due to these uncertainties and their contribution is negligiable. For the 44 systems from Drake et al. (1989) with nonsimultaneous detections in both radio and X-ray (excluding one long period system, α Aur, which would have contributed 30% of the total scatter), the scatter $\sigma_{\rm DSL}$ of the measured $\log L_6$ values about the least-squares fit to the same 44 points is 0.45, which corresponds to a variation of a factor of 2.8 in $L_{\rm radio}$. We expect the scatter to decrease systematically with smaller sample sizes, since a least-squares fit, by definition, minimizes σ, and therefore the r.m.s. scatter of a small sample about a fit to that sample will be less than the scatter of the same sample about the "true" relationship defined by a larger population. Indeed, a set of 10 systems chosen at random from the 44 systems from Drake et al. (1989) produced a scatter $\sigma'_{\rm DSL}$ of 0.42. This suggests that the values of the scatter for simultaneous and nonsimultaneous measurements are not significantly different.

In terms of the theoretical framework described above, there are three possible explanations for the similarity of $\sigma_{\rm sim}$ and $\sigma_{\rm DSL}$. First, the scatter of $\langle \log L_{\rm radio} \rangle$ among different systems with similar values of $\langle \log L_x \rangle$ could be more important than the variations $\Delta \log L_{\rm radio}$ and $\Delta \log L_x$ of individual systems. Second, $\Delta \log L_{\rm radio}$ and $\Delta \log L_x$ for an individual system could be uncorrelated or poorly correlated. Third, $\Delta \log L_{\rm radio}$ and $\Delta \log L_x$ could be well correlated, but this correlation could have a significantly different slope than that of the correlation of $\langle \log L_{\rm radio} \rangle$ and $\langle \log L_x \rangle$. The third possibility seems unlikely, since it would probably require two different mechanisms for correlating mean radio and X-ray luminosities and deviations from those means. Thus the first and second possibilities are most likely. To distinguish between these two explanations would require long-term simultaneous observations of individual systems.

3.5. Correlation of UV/XUV and X-ray/radio emission

Empirical correlations between radiation emitted at different wavelengths from stellar chromospheres and coronae are well established on the basis of nonsimultaneous data. For example, several studies (Ayres et al. 1981; Walter 1982; Oranje et al. 1982; see also Jordan & Linsky 1987) have shown that, as the energy loss from the chromospheres of active stars increases, the total energy loss from the overlying transition region and corona increases more rapidly with increasing plasma temperature. Schrijver (1987) showed that when the so-called *basal* flux is subtracted from chromospheric lines, the power-law correlations among chromospheric, transition region and coronal energy losses become much tighter. Hammer et al. (1982) called attention to the less rapid decrease of the mechanical (magnetic and non-magnetic) energy flux (F_m) with chromospheric pressure (p_{chr}), i.e., $d(\log F_m)/d(\log p_{chr}) < 1$, while the total energy loss (F_{loss}) from the transition region and corona increases faster than the transition region pressure p_{tr}. This difference in dependence of the energy balance terms on the local pressure for the different temperature regimes in a stellar atmosphere, i.e., $d(\log F_m)/d(\log p_{chr}) < d(\log F_{loss})/d(\log p_{tr})$, appears to be generally valid and is consistent with available chromospheric and coronal models (Jordan 1980; Vernazza et al. 1981; Rosner et al. 1978). Moreover, Hammer et al. (1982) demonstrated that one of the consequences of this inequality is that the observed trend of energy losses from the atmospheres of active stars is a necessary requirement for the stability of the entire chromosphere/transition region/corona system.

Our data set permits us to test these empirical correlations using simultaneous observations. To avoid systematic errors in the luminosities due to the uncertain distances, we use the distance-independent fractional luminosities, L_λ/L_{bol}, to search for correlations among the X-ray, UV, XUV and radio data sets. The fractional X-ray luminosities L_x/L_{bol} are plotted in Fig. 6 versus UV emission line fractional luminosities L_λ/L_{bol}.

The linear log–log or power-law relation between the transition region and X-ray fractional luminosities, previously obtained from nonsimultaneous data, is here confirmed with simultaneous data for 10 systems. The Mg II h + k and other chromospheric line fractional luminosities show the largest spread and weakest dependence upon X-ray luminosities (bottom panel of Fig. 5). In the case of the Mg II, $h + k$ line luminosities, the correlation is rather poor also because the luminosity range covered is too small, so that it is impossible to derive any reasonable conclusion. Weighted least-squares regression fits to the log–log data give the mean slopes 1.02 ± 0.21 and 1.36 ± 0.21 and correlation coefficients 0.68 and 0.89 for the co-added chromospheric (Mg II + O I + C I) and transition region (Si IV + C IV + N V) line fractional luminosities, respectively. Table 10 summarizes the derived slopes and correlation coefficients for each UV line. The weight attributed to each data point is $w_i = q_i \sqrt{1/\sigma_{y_i}}$, where σ_{y_i} is the standard deviation of the $\log(L_x/L_{bol})$ data derived from the uncertainty in the X-ray count-rates, while q_i is a quality factor we have assumed for each spectrum depending on its S/N ($q_i = 1$ for SV Cam, WW Dra and Z Her spectra, and $q_i = 2$ for the other systems).

The XUV fractional luminosities (L_{S1}/L_{bol} and L_{S2}/L_{bol}), in the upper panel of Fig. 5, are tightly correlated with each other and with the X-ray fractional luminosities. Weighted least-squares regression fits to the log–log data give mean slopes 0.91 ± 0.17 (for L_{S2}/L_{bol} versus L_{S1}/L_{bol}), 1.02 ± 0.17 (for L_x/L_{bol} versus L_{S1}/L_{bol}), and 1.06 ± 0.18 (for L_x/L_{bol} versus L_{S2}/L_{bol}), with linear correlation coefficients 0.97, 0.95, and 0.91, respectively. In this case only the σ for the X-ray data was used to compute the weight.

The least luminous X-ray source in our sample, ζ And, systematically deviates from the correlation trends defined by the entire data set (see Fig. 5). Its chromospheric and transition region lines appear overluminous, which perhaps could be explained if a flare-like event were occurring at the time of our observations. We note, however, that ζ And is the only super-

© European Southern Observatory • Provided by the NASA Astrophysics Data System

1994A&A...284...91F

Table 10. a and b coefficients of the linear fits $\log(L_x/L_{bol})$ $= a\log(L_\lambda/L_{bol}) + b$ resulting from a weighted best fit to the data. c is the correlation coefficent, and $No.$ the number of points

Wavelength	a	b	c	$No.$
C III (1175 Å)	1.27 ± 0.18	3.60	0.97	7
N V (1241 Å)	0.98 ± 0.19	1.95	0.71	9
O I (1304 Å)	1.74 ± 0.40	5.46	0.58	8
C II (1335 Å)	1.31 ± 0.19	3.30	0.95	9
O I+C I (1356 Å)	1.16 ± 0.28	2.95	0.77	4
Si IV (1394, 1403 Å)	1.94 ± 0.30	7.02	0.90	8
C IV (1550 Å)	1.24 ± 0.19	2.53	0.89	10
He II (1640 Å)	1.52 ± 0.22	4.47	0.96	9
C I + [O III] (1658 Å)	1.93 ± 0.31	6.81	0.86	9
Si II (1808, 1817 Å)	2.87 ± 0.41	11.44	0.96	7
Al III (1855 Å)	1.80 ± 0.35	6.92	0.95	4
Mg II $h + k$ (2795, 2802 Å)	0.71 ± 0.91	-1.18	0.13	8
S1 (69-146 Å)	1.02 ± 0.17	1.07	0.95	11
S2 (113-200 Å)	1.06 ± 0.18	1.24	0.91	10
3.6 cm	0.46 ± 0.21	4.96	0.81	10

giant in our limited sample of RS CVn systems, so that we can not ascertain whether the observed excess is connected with its luminosity class, and the time coverage is not sufficiently extended to verify the flare hypothesis.

No clear correlation is apparent between either L_{S1}/L_{bol} or L_{S2}/L_{bol} and fractional luminosities at 3.6 cm, $L_{3.6cm}/L_{bol}$, but it may possibly be hidden by the rather large spread in the data (Fig. 6). The $L_{S1}/L_{3.6}$ and $L_{S2}/L_{3.6}$ ratios for the five systems with simultaneous XUV and microwave observations span the range from $10^{13.3}$ to $10^{14.7}$ with mean value $10^{13.9\pm0.6}$.

Because only 10 systems were observed simultaneously, the derived correlations may not show less scatter than those derived from nonsimultaneous observations, but they should have more accurate slopes as they are based on simultaneous observations of chromosphere, transition region and coronal plasmas in the atmospheres of active stars, which are generally variable. As for the radio data presented in the preceding section, the intrinsic data spread that we observe attributable to temporal variability does not exceed the data spread among the different stars. We may conclude, therefore, that while nonsimultaneous data are adequate to derive qualitative trends in classes of objects between luminosities in different bandpasses, accurate energy balance calculations for specific objects should rely on simultaneous observations. Actually, the simultaneous observations of RS CVn systems presented in this paper show power-law dependencies of the fractional luminosities L_x/L_{bol} versus $L_{C\ IV}/L_{bol}$ (1.24 ± 0.19) and $L_{3.6}/L_{bol}$ versus $L_{C\ IV}/L_{bol}$ (3.73 ± 0.14), respectively, differ somewhat from those derived from a large sample of active binary giant and dwarf stars observed at X-ray and radio wavelengths years apart in time (1.59 ± 0.24 and 2.18 ± 0.27, respectively) by Drake et al. (1989).

4. Conclusions

The main results of our coordinated VLA, ROSAT and IUE observations may be summarized as follows:

1. Observations of TY Pyx during the first 3 of 4 days suggest that quiescent radio emission in RS CVn systems, defined as low-level emission with no obvious signs of flaring, can be characterized by a relatively constant level on time scales of up to 7 hours, but that this level can vary by a factor of 2 between consecutive days. If quiescent emission is the sum of many small flares, this implies either that a typical small flare lasts for at least several hours, or that the occurrence of individual flares is correlated over a similar time scale. The most probable explanation for the enhanced radio emission on 1990 Nov 12 is a flare.

2. The detection of a radio flare in its decay phase from EI Eri, with no associated change in the simultaneous X-ray count rate, points toward a poor correlation between radio and X-ray flares on RS CVn systems, similar to the lack of correlation that has been noted for dMe flare stars. While a gyrosynchrotron mechanism for the flare emission is not ruled out, the large source size that would be required (roughly four times the orbital separation of the two components in diameter, or larger if the actual flare peak preceded the start of our observations) makes a coherent mechanism, such as an electron cyclotron maser, a more likely explanation. A coherent mechanism involving efficient radio emission from a small number of electrons, which have negligible impact on the overall X-ray emission, could also account for the lack of correlation between radio and X-ray emission.

3. Despite the poor correlation of flare emission, and the uncertainty as to how closely variations in the quiescent radio and X-ray emission of an individual system are correlated, our simultaneous VLA and ROSAT observations support the existence of the correlation between the centimeter radio and soft X-ray luminosities of RS CVn systems proposed by

© European Southern Observatory • Provided by the NASA Astrophysics Data System

1994A&A...284...91F

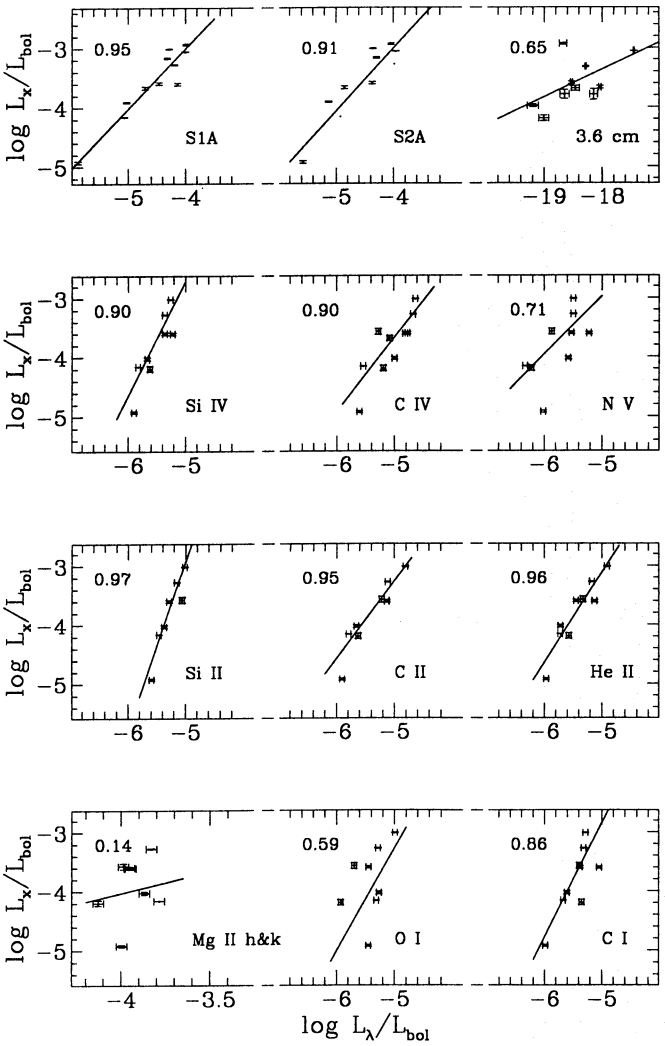

Fig. 5. L_x/L_{bol} versus fractional luminosities in the S1A and S2A XUV bandpasses of the WFC, in the 3.6 cm radio band, and in typical chromospheric and transition region lines from simultaneous or nearly simultaneous observations with ROSAT, IUE, and the VLA. The correlation coefficients are given in the upper left corner of each plot

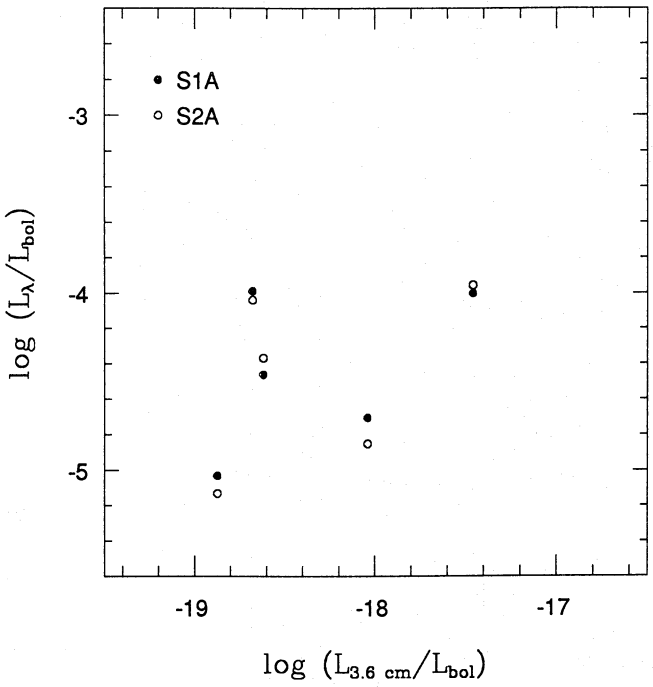

Fig. 6. The fractional luminosities in the S1A (closed circles) and S2A (open circles) XUV bandpasses of the ROSAT WFC versus the corresponding ($L_{3.6}/L_{bol}$) luminosities

Drake et al. (1989) on the basis of their noncontemporaneous data. Both the slope ($L_{3.6} \sim L_x^{0.96\pm0.24}$) and the r.m.s. scatter ($\delta(\log L_{3.6}) \sim 0.40$) of the relationship are consistent with the results of nonsimultaneous X-ray and 6 cm radio observations. There are two possible explanations for why the r.m.s. scatter of the simultaneous measurements is not significantly lower than that of the nonsimultaneous data. Either the values of $\log L_{\rm radio}$ and $\log L_x$ for individual systems are weakly correlated, or the scatter about the correlation $\langle L_{\rm radio}\rangle \sim \langle L_x\rangle^m$ for both simultaneous and nonsimultaneous measurements is dominated by the deviations of individual systems from this relationship, so that the variations $\Delta \log L_{\rm radio}$ and $\Delta \log L_x$ of $\log L_{\rm radio}$ and $\log L_x$ about their mean values, which are uncorrelated for nonsimultaneous measurements, do not contribute significantly to the scatter in either case.

4. Simultaneous microwave, X-ray, XUV and UV observations of active stars are presented for the first time. We confirm the linear log–log or power-law dependence of X-ray, transition region and chromospheric emission previously derived from nonsimultaneous data, although our slopes differ somewhat from the previous values. No correlation is found, however, between microwave and XUV energy emission.

5. Although the mean correlations between emission at different wavelengths derived from our simultaneous observations of a limited sample of RS CVn systems do not differ significantly from the empirical correlations based on nonsimultaneous observations of a larger sample of stars, we note that individual energy loss rates measured from simultaneous observations often deviate significantly from the mean relations. Thus one should base model calculations for specific stars on measured simultaneous data.

As pointed out by the referee, this paper highlights the continuing need for long-term systematic observations of active stars simultaneously at all wavelengths from the radio to x-rays. These studies should cover many orbital and rotational periods with minimal data gaps to separate the spatial inhomogeneity from temporal variability and to determine the time scales for variability and the appropriate energy budgets. Clearly more work must be done to understand the relationship between quiescent and flare emission, thermal and nonthermal processes, and the physics that underlies the flux-flux relationships of different spectral features. We therefore encourage more simultaneous observing campaigns that are focussed to address these important questions.

© European Southern Observatory • Provided by the NASA Astrophysics Data System

1994A&A...284...91F

Acknowledgements. This work was supported by Interagency Transfer W-17,772 from NASA to the National Institute of Standards and Technology and by NASA grants NAG5-82, NAG5-1792, and NAG5-1797 to the University of Colorado. The Italian coauthors acknowledge support for stellar activity research at Catania University and Astrophysical Observatory by the Ministero dell'Università e della Ricerca Scientifica e Tecnologica (MURST), the Consiglio Nazionale delle Ricerche: Gruppo Nazionale di Astronomia (CNR: GNA) and the Agenzia Spaziale Italiana (ASI).

The ROSAT WFC and IUE projects are supported by the U.K. Science & Engineering Research Council (SERC), the IUE project is jointly supported by NASA and the European Space Agency (ESA).

We thank Dr. M. Güdel and Dr. S. Skinner for many helpful discussions concerning the analysis of the radio observations. We also thank Dr. E. Guinan for permission to quote UV line flux data from his IUE spectrum of V 711 Tau obtained within the RIASS program and thank Dr. R. Pallavicini for his helpful comments on the manuscript.

References

Ayres, T. R., Marstad, N. C., & Linsky, J. L. 1981, ApJ, 247, 545
Ayres, T. R. et al. 1993, in preparation.
Brown, A., Wood, B. E., Linsky, J. L., Bromage, G. E., Kellett, B. J., & Wonnacott, D. X. 1993, ApJ, to be submitted.
Byrne, P. B. 1992, in Surface Inhomogeneities on Late-Type Stars, ed. P. B. Byrne & D. J. Mullan (Berlin: Springer-Verlag), 3
Chiuderi Drago, F., & Franciosini, E. 1993, in Physics of Solar and Stellar Coronae: G.S. Vaiana Memorial Symposium, ed. J.L. Linsky & S. Serio (Dordrecht: Kluwer), 405.
Cruddace, R.G., Hasinger, G., Trümper, J., Schmitt, J.H.M.M., Hartner, G.D., Rosso, C., & Snowden, S.L. 1989, *Experimental Astronomy*, 1, 365.
Dempsey, R. C., Linsky, J. L., Fleming, T. A., & Schmitt, J. H. M. M. 1993a, ApJS, 86, 599.
Dempsey, R. C., Linsky, J. L., Schmitt, J. H. M. M., & Fleming, T. A. 1993b, ApJ, 413, 333.
Doyle, J. G., van den Oord, G. H. J., & Kellett, B. J. 1992, A&A, 262, 533.
Drake, S. A. 1992, private communication.
Drake, S. A., Simon, T., & Linsky, J. L. 1989, ApJS, 71, 905.
Drake, S. A., Simon, T., & Linsky, J. L. 1992, ApJS, 82, 311.
Dulk, G. A. 1985, ARA&A, 23, 169
Dulk, G. A., & Marsh, K. A. 1982, ApJ, 259, 350
Eaton, J. A. 1992, in Surface Inhomogeneities on Late-Type Stars, ed. P. B. Byrne & D. J. Mullan (Berlin: Springer-Verlag), 15
Fekel, F. C., Quigley, R., Gillies, K., & Africano, J. L. 1987, AJ, 94, 726
Hall, D. S. 1976, in IAU Colloquium 29, Multiple Periodic Variable Stars, ed. W. S. Fitch (Dordrecht: Reidel), 287.
Hammer, R., Linsky, J. L., & Endler, F. 1982, in Advances in Ultraviolet Astronomy: Four years of IUE Research, NASA CP 2238, 268.
Johnston, K. J., Wade, C. M., Florkowski, D. R., & de Vegt, C. 1985, AJ, 90, 1343
Jordan, C. 1980, A&A, 86, 335
Jordan, C., & Linsky, J. L. 1987, in Exploring the Universe with the IUE Satellite, ed. Y. Kondo (Dordrecht: Reidel), 259.
Karpen, J. T., et al. 1977, ApJ, 216, 479
Kent, B. J., Reading, B. H., Swinyard, B. M., Graper E. B., & Spurrett, P. H. 1990, in EUV, X-Ray, and Gamma-Ray Instrumentation for Astronomy, Proc. SPIE, 1344, 255.
Kundu, M. R., Pallavicini, R., White, S. M., & Jackson, P. D. 1988, A&A, 195, 159
Kürster, M. et al. 1993, in preparation.
Kürster, M., Schmitt, J. H. M. M., & Fleming, T. A. 1992, in Seventh Cambridge Workshop on Cool Stars, Stellar Systems, and the Sun, ed. M. S. Giampapa & J. A. Bookbinder (San Francisco: Astronomical Society of the Pacific), 109.
Linsky, J. L. 1992, in Surface Inhomogeneities on Late-Type Stars, ed. P. B. Byrne & D. J. Mullan (Berlin: Springer-Verlag), 113
Linsky, J. L., Fox, D., Brown, A., Dempsey, R., Schmitt, C., Schmitt, J. H. M. M., Fleming, T., Rodonò, M., Pagano, I., Neff, J. E., & Bromage, G. 1992, in Seventh Cambridge Workshop on Cool Stars, Stellar Systems, and the Sun, ed. M. S. Giampapa & J. A. Bookbinder (San Francisco: Astronomical Society of the Pacific), 106.
Majer, P., Schmitt, J. H. M. M., Golub, L., Harnden, F. R., Jr., & Rosner, R. 1986, ApJ, 300, 360
Massi, M. & Chiuderi Drago, F. 1992, A&A, 253, 403.
Melrose, D. B. 1987, in Cool Stars, Stellar Systems, and the Sun, ed. J. L. Linsky & R. E. Stencel (Berlin: Springer-Verlag), 83
Melrose, D. B. 1991, ApJ, 380, 256
Mewe, R., Gronenschild, E.H.B.M., & van den Oord, G.H.J. 1985, *Astron. Astrophys. Suppl.* **62**, 197.
Mewe, R., Lemen, J.R., & van den Oord, G.H.J. 1986, *Astron. Astrophys. Suppl.* **65**, 511.
Morris, D. H., Mutel, R. L., & Su, B. 1990, ApJ, 362, 299
Mutel, R. L., Lestrade, J.-F., Preston, R. A., & Phillips, R. B. 1985, ApJ, 289, 262
Mutel, R. L., Morris, D. H., Doiron, D. J., & Lestrade, J.-F. 1987, AJ, 93, 1220
Neff, J. E. 1992, in Surface Inhomogeneities on Late-Type Stars, ed. P. B. Byrne & D. J. Mullan (Berlin: Springer-Verlag), 54
Neff, J. E., Pagano, I., Rodonò, M., Brown, A., Dempsey, R. C., Fox, D. C., & Linsky, J. L. 1993, to be submitted to A&A.
Oranje, B. J., Zwaan, C., & Middlekoop, F. 1982, A&A, 110, 304
Pagano, I., Rodonò, M., & Neff, J. E. 1992, in Surface Inhomogeneities on Late-Type Stars, ed. P. B. Byrne & D. J. Mullan (Berlin: Springer-Verlag), 315
Pfeffermann, E. et al. 1987, in Soft X-ray Optics and Technology, ed. E.-E. Koch & G. Schmahl, Proc. SPIE, 733, 519.
Rodonò, M. 1992, in Evolutionary Processes in Interacting Binary Stars, ed. Y. Kondo, R. F. Sisteró, & R. S. Polidan (Dordrecht: Kluwer), 71.
Rodonò, M., et al. 1987, A&A, 176, 267
Rosner, R., Tucker, W. H., & Vaiana, G. S. 1978, ApJ, 220, 643
Schrijver, C. J. 1987, A&A, 172, 111
Stern, R. A., Uchida, Y., Walter, F., Vilhu, O., Hannikainen, D., Brown, A., Veale, A., & Haisch, B. M. 1992, ApJ, 391, 760
Strassmeier, K. G., Hall, D. S., Zeilik, M., Nelson, E., Eker, Z., & Fekel, F. C. 1988, A&AS, 72, 291
Swank, J. H., White, N. E., Holt, S. S., & Becker, R. H. 1981, ApJ, 246, 208
Trümper, J. 1984, Phys. Scripta, T7, 209.
Vernazza, J. E., Avrett, E. H., & Loeser, R. 1981, ApJS, 45, 635.
Walter, F. M. 1982, in Advances in Ultraviolet Astronomy: Four years of IUE Research, NASA Conf. Pub. 2238, 566.
Wells, A., et al. 1990, in EUV, X-Ray, and Gamma-Ray Instrumentation for Astronomy, Proc. SPIE, 1344, 230.
White, G. L., Lestrade, J.-F., Jauncey, D. L., Phillips, R. B., Preston, R. A., & Reynolds, J. E. 1990, AJ, 99, 405

This article was processed by the author using Springer-Verlag LaTeX A&A style file version 3.

© European Southern Observatory • Provided by the NASA Astrophysics Data System